Novel Approach to Constructing an Ultra Low Cost Flowcell Biosensor

THESIS

Presented to the Faculty of the Department of Physics and Astronomy
in Partial Fulfillment of the Major Requirements
for the Degree of

BACHELOR OF SCIENCE IN
PHYSICS

Jeffery Summers

May 2019

Novel Approach to Constructing an Ultra Low Cost Flowcell Biosensor

Jeffery Summers

Signature of Author:

Department of Physics & Astronomy

May 2019

Certified by:

Dr. William Robertson

Department of Physics & Astronomy

Thesis Supervisor

Accepted by:

Dr. Ronald Henderson

Professor of Physics & Astronomy

Chair, Physics & Astronomy

ABSTRACT

In this thesis we present our approach to constructing an ultra low-cost flowcell biosensor. Our sensor is capable of detecting changes in index of refraction on the order of 10^{-5}, showing that it is well suited for not only index testing but also for surface loading type processes where binding between molecules may occur. Our sensor utilizes 3D printed parts, a one dimensional photonic crystal coupled to a glass prism (rather than a traditional SPR metal-film-prism coupling system), and a CCD to operate. Bloch Surface Waves (BSWs) can be excited in the outer layer of our multilayer by coupling an incident laser beam to the prism-multilayer structure and the position of the BSWs can be tracked by analyzing the reflected beam. By using this method we are able to bring the cost of manufacturing the sensor to about $100, excluding the photonic crystals which can be fabricated commercially. The largest cost of our system is the CCD used to collect data.

TABLE OF CONTENTS

LIST OF FIGURES

I. INTRODUCTION

Flowcell sensors have many applications; disease detection, refractive index measurements and measurements of reactivity to name a few. These sensors have been operating on the basis of electromagnetic surface phenomena for decades. Most flowcells on the market work by exploiting surface plasma oscillations (SPOs). These oscillations are highly sensitive to changes in the optical properties of the adjacent medium and follow from Maxwell's equations when the dielectric functions of each medium satisfy the relation [**?**]

$$\frac{\epsilon_{spo}}{\epsilon_{adjacent}} < -1$$

Metals like aluminum, copper, gold, and silver have negative dielectric functions at wavelengths in the red/infrared [], so films of these metals are used as to generate SPOs in most flowcell sensors via a process known as Surface Plasmon Resonance (SPR). An SPR system utilizes light-prism coupling to excite the surface electrons on a thin metal film deposited on the hypotenusal face of the prism. A dark band representing the photons absorbed by the

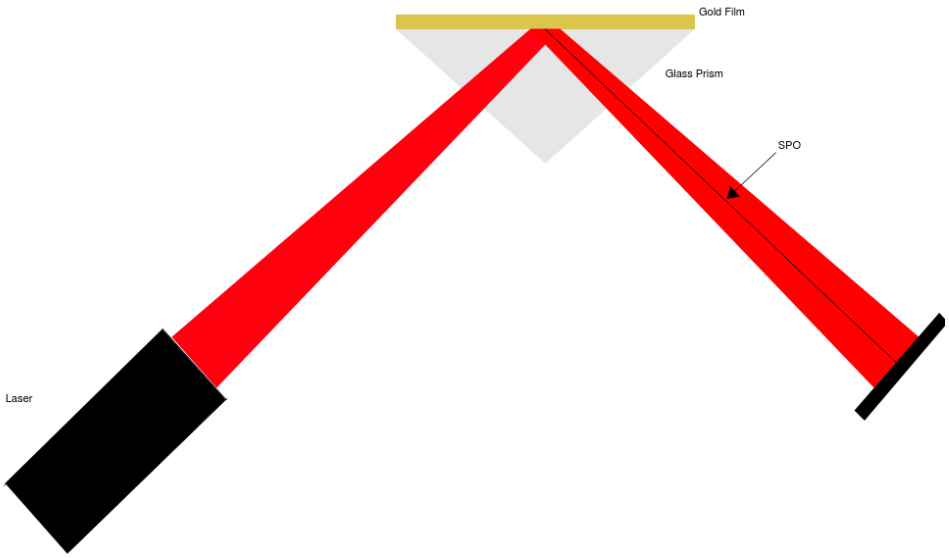

Figure 1: Surface Plasmon Resonance setup

surface electrons appears on the reflected beam image as seen in figure 1. There are quite a few drawbacks for using metal films, however. Metals are highly reactive so each time an SPR system is used a new prism must be used. These films also require particular wavelengths of incident light to excite the oscillations. Rather than using metal films, one-dimensional photonic crystals, or multilayers, can be designed to exhibit the phenomenon of surface electromagnetic waves (SEWs) or Bloch surface waves (BSWs), named after the physicist Felix Bloch who was famous for working with periodic systems. These surface waves have the same practical application as SPOs.

Multilayers overcome both of the shortcomings of metal films listed here. They can be designed to work for any wavelength and are typically made of nonreactive glass. In addition to these benefits, we expect that our 3-D printed and multilayer-based flowcell sensor will be more sensitive and precise with its measurements and be far cheaper to both build and maintain compared to traditional SPR sensors.

To take measurements with our sensor we look at the reflected image of incident laser light which has been coupled into the prism-multilayer interface to produce a BSW in the terminating layer. Our multilayer is designed to trap incident light in the last layer at a special angle; this results in a dark band in our reflected image. A diagram of the sensor is shown below.

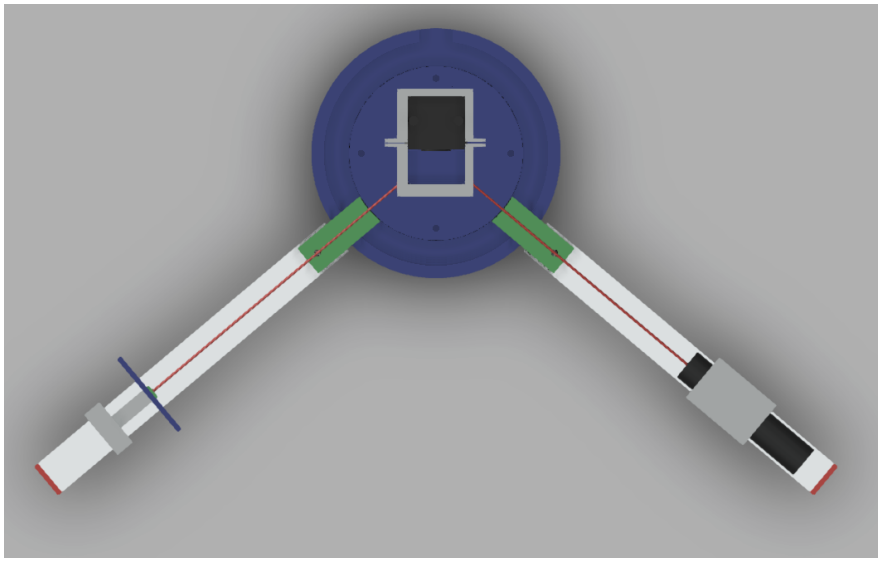

Figure 2: The laser on the right side of the image couples into the prism-multilayer structure atop the centerpiece and is then reflected into a CCD where data can be taken.

As fluids or gases are put into the flowcell chamber the index of refraction, n_c, changes. The condition for total internal reflection, found from Snell's law, for the interface between a glass prism and some transmitting medium whose index of refraction varies with time is given by:

$$\sin\theta_c = \frac{n_c(t)}{n_g}$$

We obtain an expression for the angle of reflection as a function of time by the Law of Reflection:

$$\theta_r(t) = \arcsin\frac{n_c(t)}{n_g}$$

Note that this expression is only valid for a single interface and hence does not accurately reflect our setup as we use a multilayer that behaves much differently than a single interface. With that said, this expression for θ_r does capture

the essence of our setup; the reflected angle (this is equivalent to the position of the surface mode) is a dependent on the index of refraction of the chamber. Using this fact we can associate variations in the flowcell chamber's index of refraction with differences in the BSWs angular position. These angular differences can be calculated by tracking the variation in the position of the dark band in the reflected image. A detailed analysis relating a shift in pixels on the CCD to the angular variation of the surface mode is listed in the methods section.

To use this device for disease detection, or to detect any sort of biological binding process, the multilayer must have the binding agent in question deposited onto the outer layer. The characteristic of the surface mode is first captured with just the binding agent and an empty (or water filled) flowcell chamber. After acquiring the characteristic of the surface mode the molecules to be binded are then flushed through the chamber and if binding occurs the surface mode's characteristics will be different than before.

II. Experimental Design

The process of design for this experiment relies heavily on the use of a 15 milimeter right prism and our photonic crystal. The photonic crystal is composed of 3 bilayers of TiO2 and SiO2. The dielectric function of TiO2 is taken as $\epsilon_{TiO2} = 4.84 + 0.0007i$ and the dielectric function of SiO2 is taken as $\epsilon_{SiO2} = 2.1316 + 0.0001i$.

It should be noted that the imaginary parts of each dielectric function may not be accurate and have been included to introduce some form of loss that fits the results of prior experiments []. Figure 3 illustrates the structure of the multilayer. The basic design of the sensor is split into three different parts: the primary stage, two beams, and the flowcell stage. The primary stage acts as the center about which the incident beam can be coupled to the prism and then reflected. One of the two beams holds our laser and a focusing lens while the other holds the CCD and captures the reflected beam. The flowcell stage is a modular piece that is attached to the primary stage with four bolts, the prism, multilayer, and flowcell chamber are all strapped together on this stage. The modular nature of this piece of the sensor is very valuable since many designs can be used to achieve the same goal and it only takes about an hour to print off each stage.

Figure 3: An illustration of the photonic crystal used in our sensor

To operate the sensor both beams need to be oriented at the *coupling angle*. When the chamber is filled with water this angle is about 66° from the surface of the prism. This is a rather extreme angle and so the parts that connect the beams to the rim of the primary stage are fashioned to allow the beams to pivot about their connection points. This allows the beams to be oriented at extreme angles with respect to the surface of the prism.

III. Methods

To collect data from our biosensor we first prepare the flowcell chamber with the correct substrate or liquid that acts as our reference point for measuring changes in optical properties. After the chamber is prepared we then turn on the beam and rotate it until the special angle is reached.

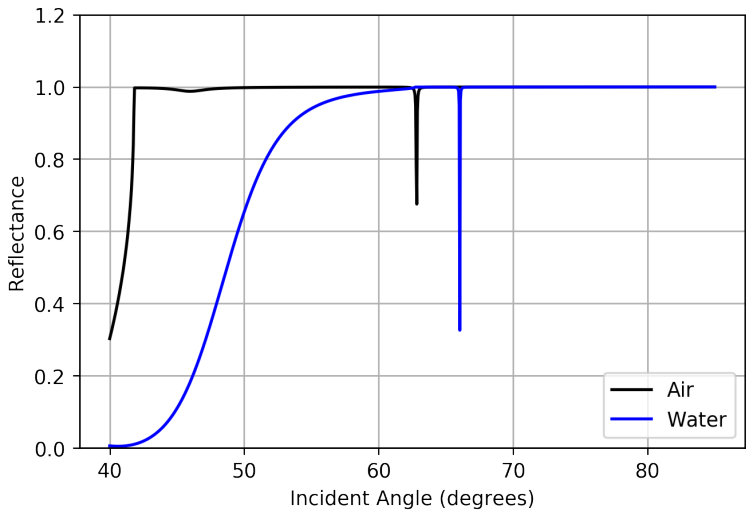

As the index of refraction inside the flowcell chamber changes the dark band will translate left or right in our reflected image, depending on whether the index is increasing or decreasing. The shift in location of the band, in pixels, corresponds to an angular shift in the part of the reflected beam giving rise to the dark band. This is shown clearly in ?? as we see that a change from an index of 1.00 (air) to 1.33 (water) corresponds to an angular shift of about 3°.

Using the calculated data we can build a model to relate the index of refraction in the chamber to a shift in pixels on our CCD. To construct this relation we require Snell's law and some geometry. Using the classic formula for arclength and the diagram below we find:

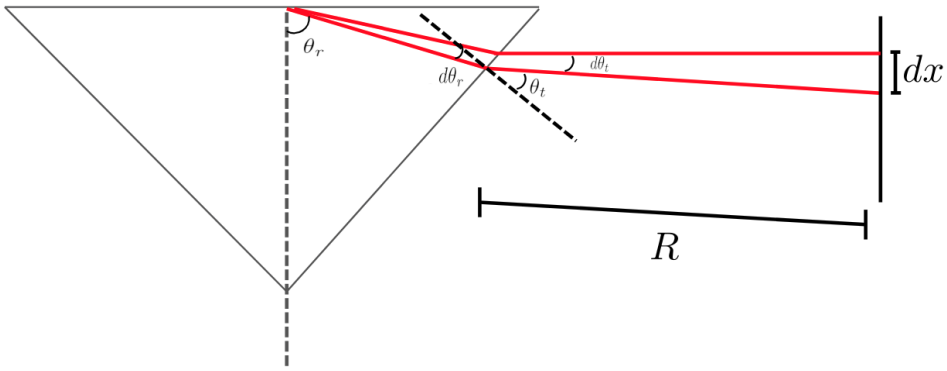

$$dx = Rd\theta_t$$

Using Snell's law we find

$$\theta_t = \arcsin(\sin(n_g \theta_r))$$

Which implies that

$$\begin{aligned} d\theta_t &= d\left(\arcsin\left(n_g \sin\theta_r\right)\right) \\ &= \frac{n_g \cos\theta_r}{\sqrt{1 - n_g^2 \sin^2(\theta_r)}}\, d\theta_r \end{aligned}$$

This leaves us with the relation between pixel shift and angular shift:

$$dx = \frac{R n_g \cos\theta_r}{\sqrt{1 - n_g^2 \sin^2(\theta_r)}}\, d\theta_r \tag{1}$$

Numerically we can determine the relationship between the reflected angle and the index inside the chamber. I wrote a python program to do just that for our multilayer, assuming the chamber is initially filled with water, and a graph of mode position (θ_r) vs index of refraction is plotted below.

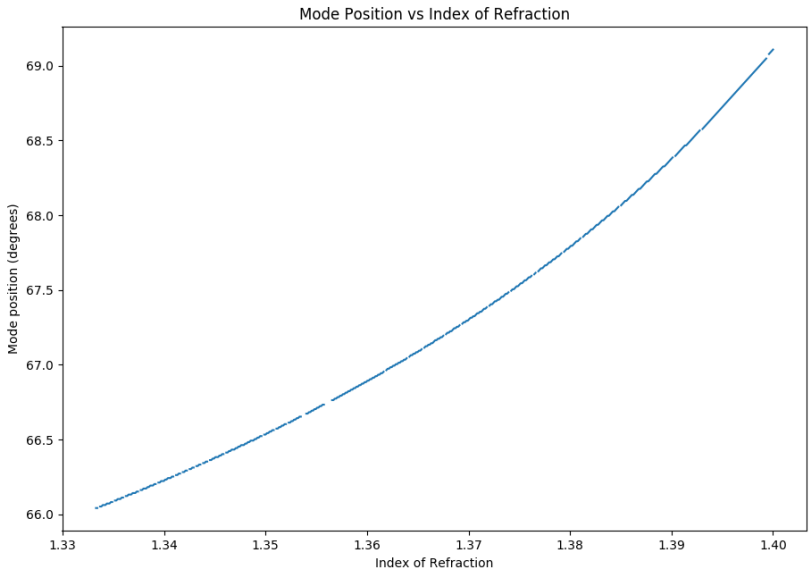

Figure 4: The theoretical relation between the angular position of the mode and the index of refraction inside the flowcell chamber.

IIII. RESULTS

The table below lists the mixtures of ethanol used to test for a change in index of refraction. The plot below shows the different indices of refraction corresponding to mixture A being injected over the interval $[25, 55]$. Similarly mixture B was injected over the interval $[70, 90]$, and mixture C over $[100, 150]$. After the mixtures have time to settle in the chamber, they are flushed out with the same deionized water used to indicate the baseline mode position. Upon injecting a mixture with a higher index into the chamber we notice that the mode position shifts, as expected.

Using this data we can acquire a quantitative value for how large of an index shift results from a shift in one pixel. All of the mixtures used for testing have indices between 1.3380 and 1.3464, meaning that when the pixel shift of each mixture is plotted against the index of each we should expect a linear graph (see Figure 4) since small variations in reflected angle will yield a proportional shift in pixels. By extrapolating the data provided in the figure below we that a shift in one pixel corresponds to a shift of about 0.0018 in index of refraction. At this level of sensitivty the exceeds the necessary sensitive to detect surface loading [?].

Mixtures	A	B	C
Ethanol (ml)	10.0	20.0	30.0
Water (ml)	100.0	100.0	100.0
Index	1.3380	1.3418	1.3450
Pixel Shift	80.0	135.0	245.0
Change in Index	0.0049	0.0052	0.0119

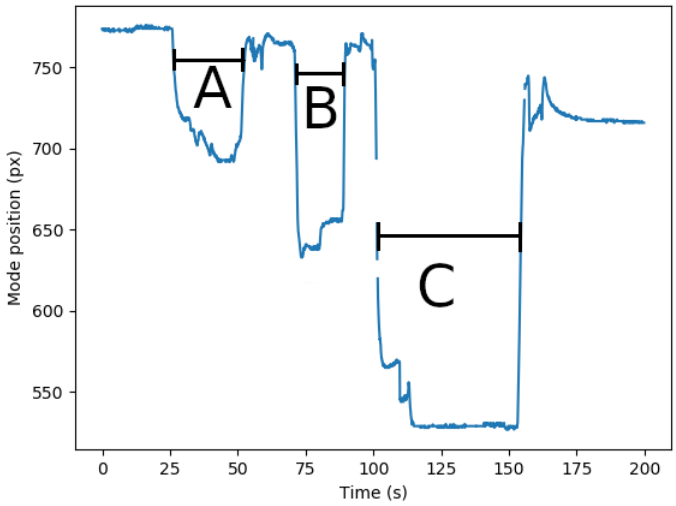

Figure 5: Index shift measurements for ethanol.

Mixtures	A	B	C
Acetone (ml)	10.0	20.0	30.0
Water (ml)	100.0	100.0	100.0
Index	1.3384	1.3430	1.3464
Pixel Shift	111.5	206.0	292.5
Change in Index	0.0052	0.0098	0.0132

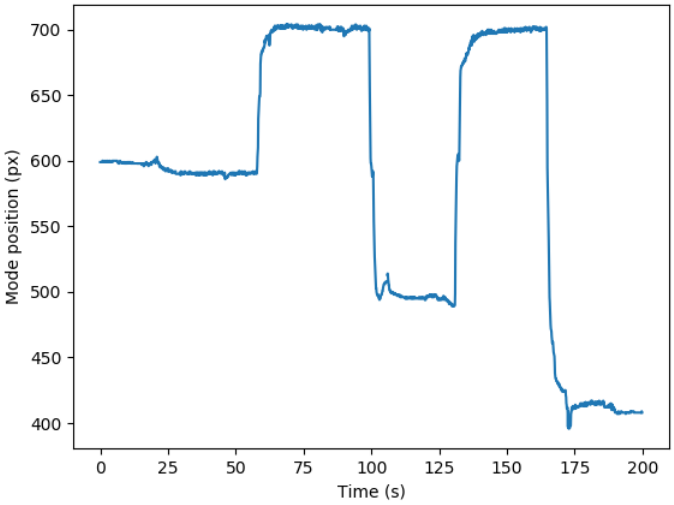

Figure 6: Index shift measurements for acetone.

Mixtures	A	B	C
70% Isop Alc. (ml)	10.0	20.0	30.0
Water (ml)	100.0	100.0	100.0
Index	1.3398	1.3412	1.3447
Pixel Shift	84.5	164.5	223.0
Change in Index	0.0066	0.0080	0.0115

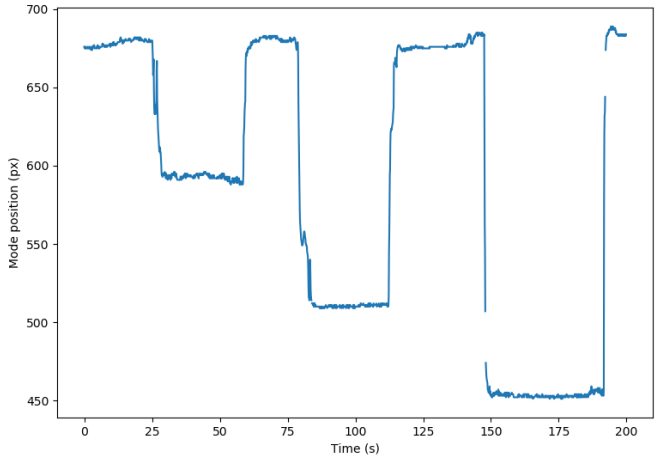

Figure 7: Index shift measurements for 70% isopropyl alcohol.